Numerical modeling of copper macro-segregation in the binary alloy Al-4Cu

Sara BENMAZIANE[1*], *Omar* BEN LENDA[1], *latifa* ZERROUK[1], and *Elmadani* SAAD[1,2]

[1]Laboratory of Physico-Chemistry of Processes and Materials, Hassan 1st University, Faculty of Sciences and Technology of Settat, Settat, Morocco
[2]Health Science and Technology Research Laboratory, Hassan 1st University, Settat, Morocco

Abstract. In this paper, the modeling of the solidification of Al-4Cu alloy was studied. The calculation code is developed to model the equiaxed globular solidification of the Al-4Cu alloy in a square mold. The mold walls are subjected to constant temperatures and the velocity components are equal to 0, the exchange coefficient 'H' between the interface of the melt and the mold is estimated at 500 W/(m^2 K) and the initial melt temperature 'T_0' is equal to 900 K. The resolution method used is finite differences, the upwind scheme for convective terms, and the space-centered scheme for diffusive terms. The calculated profiles are temperature, solid fraction, concentration and macro-segregation of copper. At the beginning of cooling, the solidification of the Al-4Cu alloy started in the four corners of the plate. The grains formed at the walls could not move in the studied surface. With cooling time, the solidification of the casting developed rapidly in the lower part; because, the grains formed away from the walls sedimented and accumulated in this part of the plate. On other hand, the liquid was located mainly in the upper part. The segregation of copper in the two-phase mixture is due to its continuous rejection from the solid to the liquid.

1 Introduction

During the cooling of alloys several phenomena are involved, such as phase change, heat and mass transfer and segregation of chemical elements, ...etc. In order to understand and analyze the complex phenomena that occur, several calculation codes have been developed by researchers or industrial companies.

The solidification of aluminum alloys is widely studied due to their wide use in several sectors such as transportation, aeronautics and construction. Aluminum alloys are characterized by an equiaxed globular structure. We can consider that the grains of this structure have a simple spherical morphology which confers interesting properties to metallic alloys [1–3].

In the literature, several works have been carried out on the modeling of solidification phenomena of aluminum alloys. First, the model developed by Beckermann et al. is cited. They are based on the volume-averaging approach of the two phases, i.e. the liquid and the solid. Each phase is treated separately, but the interactions between them are considered explicitly. Beckermann's team solved simultaneously the transport equations for the liquid

* Corresponding author: sarabenmaziane@gmail.com

and the solid. Their model allowed a rigorous description of several phenomena at the microscopic and macroscopic scales [4–10]. Nevertheless, this model has several inconveniences; for example, the absence of a real nucleation model, detailed heat transfer and density coefficients, etc., are cited.

This model has been succeeded by other works in order to propose a more complete model. Among the latter, mention should be made of the work developed by Ni and Incropera in which they established a link between the liquid and solid phases. The published model took into account solutal undercooling, nucleation, stereological characteristics of the solid/liquid interface, movement of solids as floating or settling crystals, and shrinkage [11,12].

Ludwig and Wu treated the globular equiaxed solidification always based on the volume averaging approach of the two phases. The simulation of the equations of the two phases treated separately allowed to describe nucleation, grain evolution, flow convection, sedimentation, solute transport and macrosegregation [13,14].

Tveito et al, in turn proposed a simpler model describing equiaxed solidification in order to avoid the difficulty of modeling an equiaxed grain. This three-phase model is based on the volume average method. It allows to describe the influence of grain morphology on macro-segregation [15,16].

In order to predict macrosegregation and shrinkage cavity Ren et al used a four-phase dendritic solidification model coupling several phenomena such as equiaxed grain growth and sedimentation, thermo-solutal buoyancy and shrinkage formation.... Their model was able to predict the impact of the initial mold temperature on macro-segregation and equiaxed grain growth [17].

This paper focuses on the globular solidification of alloys, and more precisely Al-4Cu in a 2D cavity. The calculation code is based on the finite difference resolution method. Another approach was developed in this study, replacing the momentum equation with stream functions and vorticity. First, the equations of the stream functions, vorticity, and temperature were solved; then, the outputs of the previous equations were used to find the fraction of solid and the concentration of copper.

2 Description of model

2.1 General assumptions

Several hypotheses are established to model the solidification of Al-4Cu alloy. It is assumed that the mold is instantly filled with melt and no feeding is performed during the cooling of the plate-mold system. Two phases are present: solid and liquid, and the latter is considered Newtonian. These phases are represented by their volume fractions (the sum is equal to 1), and their physical properties are constant as a function of temperature. The non-slip condition is defined at the mold walls.

2.2 Description of the studied case

The conditions for simulation of Al-4Cu alloy solidification are illustrated in Figure 1. In the studied case, it was considered that Al-4Cu casting takes place in the 2D mold (not explicitly modeled). The initial temperature of melt (T_0) is equal to 900 K and that of mold (T_w) is equal to 295 K. The exchange coefficient, noted as H, between the interface of the melt and the mold is estimated at 500 W/(m^2 K). The mold is cooled by free air and at atmospheric pressure. The mesh used is 40×40 square surface elements for the vertical plate of dimension 0,2×0,2 m^2.

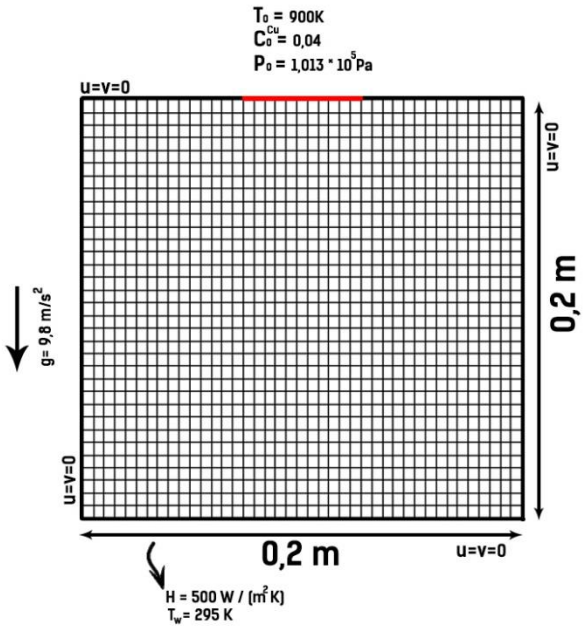

Fig. 1. Scheme of the physical model studied.

The thermophysical and thermodynamic properties of Al-4Cu alloy are reported in Table 1.

The densities, thermal conductivities, heat capacities and coefficients of thermal expansion are organized according to liquid and solid phases. They have constant and different values depending on the phase in question.

A dash is noted in the liquid phase viscosity column because it will not be used in the calculation code.

Table 1. Thermophysical and thermodynamic properties

of Al-4Cu alloy. [13,18]

Thermophysical properties		
Properties	**Liquid phase**	**Solid phase**
ρ **(kg/m^3)**	2606	2743
λ **(W/m K)**	77	153
c_p **(J/kg K)**	1179	766
β **(K^{-1})**	10^{-4}	10^{-4}
μ **(kg/m s)**	$1{,}3\text{x}10^{-2}$	___
Thermodynamic properties		
k =0,145	T_{ϕ}=933,5 K	m =-344 K

2.3 Mathematical model

The mathematical model consists in solving the equations of stream function, vorticity, temperature, solid fraction and copper concentration.

Stream function equation:

$$\frac{\partial^2\psi}{\partial x^2}+\frac{\partial^2\psi}{\partial y^2}=-\omega \tag{1}$$

Vorticity equation:

$$\frac{\partial\omega}{\partial t}+\frac{\partial\psi}{\partial y}\frac{\partial\omega}{\partial x}-\frac{\partial\psi}{\partial x}\frac{\partial\omega}{\partial y}=\frac{\mu_m}{\rho_m}\left(\frac{\partial^2\omega}{\partial x^2}+\frac{\partial^2\omega}{\partial y^2}\right)+\frac{1}{\rho_m}\left(\phi_s\rho_s\beta_s+\phi_\ell\rho_\ell\beta_\ell\right)g\frac{\partial T}{\partial x} \tag{2}$$

With: $u_\ell=\frac{\partial\psi}{\partial y}$; $v_\ell=-\frac{\partial\psi}{\partial x}$

Temperature equation:

$$\frac{\partial T}{\partial t}+\frac{\partial\psi}{\partial y}\frac{\partial T}{\partial x}-\frac{\partial\psi}{\partial x}\frac{\partial T}{\partial y}=\frac{\partial}{\partial x}\left(\frac{\lambda_m}{(\rho c_p)_m}\frac{\partial T}{\partial x}\right)+\frac{\partial}{\partial y}\left(\frac{\lambda_m}{(\rho c_p)_m}\frac{\partial T}{\partial y}\right) \tag{3}$$

Liquid fraction equation:

$$\frac{\partial(\phi_\ell\rho_\ell)}{\partial t}+\nabla.(\phi_\ell\rho_\ell v_\ell)=M_{s\ell} \tag{4}$$

Solid fraction equation:

$$\frac{\partial(\phi_s\rho_s)}{\partial t}+\nabla.(\phi_s\rho_s v_s)=M_{\ell s} \tag{5}$$

With: $M_{\ell s}=g_\alpha\left(\frac{T-T_\ell}{m}-c_\ell\right)(n\pi d_s^2)\rho_s(1-\phi_s)$ and $g_\alpha=5\times10^{-4}\,m/s$ [13]

Concentration equation:

$$\frac{\partial(\phi_\ell\rho_\ell c_\ell)}{\partial t}+\nabla.(\phi_\ell\rho_\ell v_\ell c_\ell)=C_{s\ell} \tag{6}$$

Species concentration in the solid phase:

$$\frac{\partial(\phi_s\rho_s c_s)}{\partial t}+\nabla.(\phi_s\rho_s v_s c_s)=C_{\ell s} \tag{7}$$

With: $C_{\ell s}=k\times c_\ell\times M_{\ell s}$

The thermophysical properties of the mixture are expressed based on those of the liquid and the solid. The thermal capacity and density of the mixture are formulated using the following rule:

$$\left(\rho c_p\right)_m=\phi_s\left(\rho c_p\right)_s+\phi_\ell\left(\rho c_p\right)_\ell \tag{8}$$

$$\rho_m=\phi_s\rho_s+\phi_\ell\rho_\ell \tag{9}$$

According to Ishii and Zuber [19], the viscosity of a solid-liquid mixture is expressed according to the following equation:

$$\mu_m=\mu_\ell\left(1-\frac{\phi_s}{\phi_s^c}\right)^{-2,5\phi_s^c} \tag{10}$$

With ϕ_s^c is the critical solid volume fraction from which the equiaxed crystals combine to produce a solid and rigid structure. It is equal to 0,637 [6–8].

According to Maxwell, the thermal conductivity of solid-liquid mixture can be written from the following relationship [20]:

$$\lambda_m=\frac{\phi_\ell\lambda_\ell(2\lambda_\ell+\lambda_s)+3\phi_s\lambda_s\lambda_\ell}{\phi_\ell(2\lambda_\ell+\lambda_s)+3\phi_s\lambda_\ell} \tag{11}$$

The concentration of mixture is calculated as follows:

$$c_m=\frac{c_\ell\rho_\ell\phi_\ell+c_s\rho_s\phi_s}{\rho_\ell\phi_\ell+\rho_s\phi_s} \tag{12}$$

The parameters used for the adimensioning of equations (1), (2) and (3) are:

$$X=\frac{x}{L} \quad ; \quad Y=\frac{y}{L}$$

$$\Psi=\frac{\psi}{L\sqrt{g\beta_\ell\Delta TL}} \quad ; \quad \Omega=\frac{\omega L}{\sqrt{g\beta_\ell\Delta TL}}$$

$$\tau=\frac{t\sqrt{g\beta_\ell\Delta TL}}{L} \quad ; \quad \mathcal{T}=\frac{T-T_w}{T_0-T_w} \tag{13}$$

The system of equations without dimensions is expressed as follows:

Stream function equation:

$$\frac{\partial^2 \Psi}{\partial X^2} + \frac{\partial^2 \Psi}{\partial y^2} = -\Omega \tag{14}$$

Vorticity equation:

$$\frac{\partial \Omega}{\partial \tau} + \frac{\partial \Psi}{\partial y}\frac{\partial \Omega}{\partial X} - \frac{\partial \Psi}{\partial X}\frac{\partial \Omega}{\partial y} = \frac{(1-\frac{\phi_s}{\phi_s^c})^{-2,5\phi_s^c}}{(\phi_\ell+\phi_s\frac{\rho_s}{\rho_\ell})\sqrt{\mathcal{G}r}}\left(\frac{\partial^2 \Omega}{\partial X^2} + \frac{\partial^2 \Omega}{\partial y^2}\right) + \frac{1}{\beta_\ell \rho_m}\left(\phi_s \rho_s \beta_s + \phi_\ell \rho_\ell \beta_\ell\right)\frac{\partial \mathcal{T}}{\partial X} \tag{15}$$

Temperature equation:

$$\frac{\partial \mathcal{T}}{\partial \tau} + \frac{\partial \Psi}{\partial y}\frac{\partial \mathcal{T}}{\partial X} - \frac{\partial \Psi}{\partial X}\frac{\partial \mathcal{T}}{\partial y} = \frac{1}{\mathcal{P}r\sqrt{\mathcal{G}r}}\left[\frac{\partial}{\partial X}\left(\frac{\frac{\lambda_m}{\lambda_\ell}}{\phi_\ell+\phi_s\frac{(\rho c_p)_s}{(\rho c_p)_\ell}}\frac{\partial \mathcal{T}}{\partial X}\right) + \frac{\partial}{\partial y}\left(\frac{\frac{\lambda_m}{\lambda_\ell}}{\phi_\ell+\phi_s\frac{(\rho c_p)_s}{(\rho c_p)_\ell}}\frac{\partial \mathcal{T}}{\partial y}\right)\right] \tag{16}$$

Dimensionless numbers are formulated based on the thermophysical properties of used alloy. With Prandtl's number is $\mathcal{P}r = \frac{\mu_\ell c_{p_\ell}}{\lambda_\ell}$ and the Grashof's number is $\mathcal{G}r = \frac{g\beta_\ell \Delta T L^3 \rho_\ell^2}{\mu_\ell^2}$.

2.4 Numerical method

The dimensionless equations, cited in section 2.3, are discretized by finite difference method. The upwind scheme was used for convective terms, and the centered-space scheme for diffusive terms.

The convergence criterion used for our calculation code is as follows:

$$\sum|\Psi_{i,j}^{n+1} - \Psi_{i,j}^{n}| < 10^{-6} \tag{17}$$

Edge vorticity is determined by the Taylor development of stream functions. They are expressed as follows:

$$\begin{aligned}
\Omega_{i,1} &= -2 * \frac{\Psi_{i,2}}{\Delta x^2} \\
\Omega_{i,ny} &= -2 * \frac{\Psi_{i,ny-1}}{\Delta x^2} \\
\Omega_{1,j} &= -2 * \frac{\Psi_{2,j}}{\Delta y^2} \\
\Omega_{nx,j} &= -2 * \frac{\Psi_{nx-1,j}}{\Delta y^2}
\end{aligned} \tag{18}$$

The accuracy of the calculation is significantly influenced by the density of the mesh, and more precisely the parts close to the edges of mold. The mesh density is determined based on the boundary layer theory [21]:

$$\Delta\delta \times \sqrt{\frac{\rho_\ell \times u_\ell^\infty}{\mu_\ell \times \tilde{y}}} \leqslant 1 \tag{19}$$

According to equation (19), our mesh must be fine enough to obtain very precise results. In our case, the height of the casting $\tilde{y}$ is 0,2 m and the maximum velocity u_ℓ^∞ is 0,03 m/s. Therefore, the mesh size $\Delta\delta$ of the parts close to the wall must be less than 5,8 mm. A mesh size of 5×5 mm^2 has been chosen for each element.

3 Results and discussions

The profiles of temperature, solid fraction, concentration and stream functions after 10 seconds are illustrated in Figure 2. After 10 seconds, the isotherms are symmetrical with respect to the vertical axis (fig. 2(a)). We note a maximum value in the center and a minimum value at the extremity of the plate. The cooling of the plate-mold system is essentially done by free convection heat extraction by means of air. At this stage, it can be assumed that grain sedimentation and convection driven by it is not yet significant.

According to Figure 2(b), the beginning of solidification is observed in the extremities and significantly in the four corners, but the rate of the solidified liquid phase remains low. Due to the non-slip condition assumed in section 2.1, the immediately developing Al-4Cu solid grains cannot move and remain attached to the walls of the mold.

In Figure 2(c), there is a difference in the concentration of copper in the biphasic mixture. It is observed that more the solid fraction of the phase increases, the more the phase weakens into copper and vice versa. These results can be explained by the rejection of copper in the melt during phase change from liquid to solid.

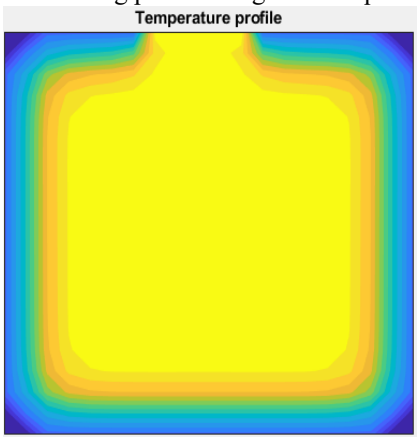

(a) 800 to 900 K

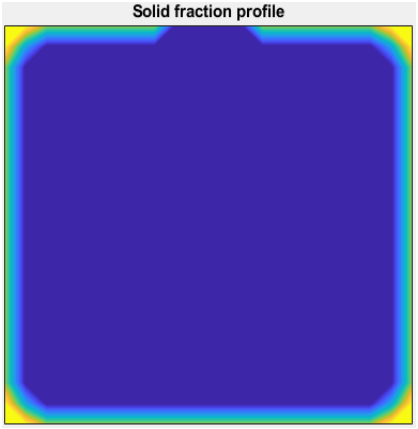

(b) 0 to 0,7

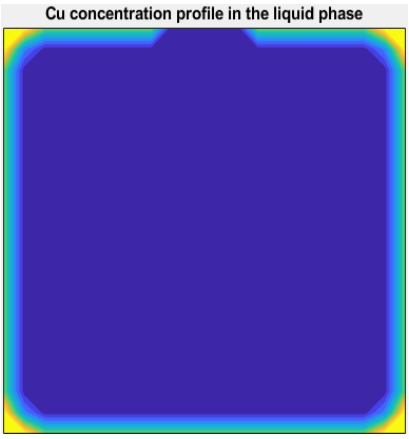

(c) 0,04 to 0,12

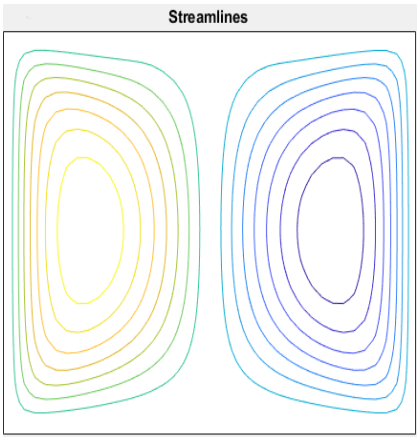

(d) 6×10^{-5} to 6×10^{-5}

Fig. 2. Temperature profiles, solid fraction, streamlines and solute concentration after 10 seconds from the start of cooling. All quantities are scaled equidistantly with yellow representing the highest value and blue the lowest value.

Figure 3 represents the profiles of the solid fraction, the streamlines and the concentration of the solute after 60 seconds from the start of cooling. According to Figure 3(a), the solidified mass is important in relation to the beginning of cooling (fig. 2(a)). Continuous cooling of our study alloy gives rise to other solid grains away from the mold walls that do not obey the non-slip condition. Over time, these grains sediment and also accumulate at the bottom of the casting, strongly modifying the profile of the solid fraction. It is observed that

the solidification in the lower corners and the bottom of the piece progresses more rapidly compared to the lateral regions.

There is a similarity between the profiles of the solid fraction and the copper concentration related by equations (4) and (5). As expected, the copper fraction is important just in the zones adjacent to the solidified ones (fig. 3(b)). This solute segregation is caused by the continuous release of solute over time from the solid to the liquid phase.

This change of phases thus creates two oppositely directed vortices, the first turning clockwise and the second turning anticlockwise, as represented in Figure 3(c).

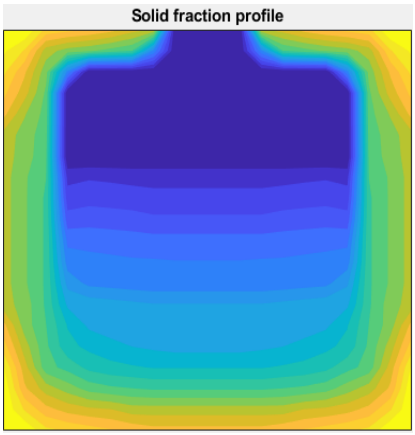

(a) 0 to 0,9

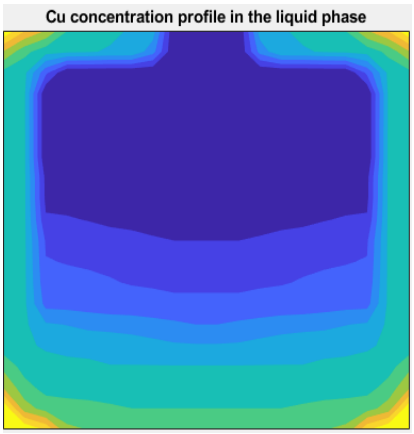

(b) 0,04 to 3,2

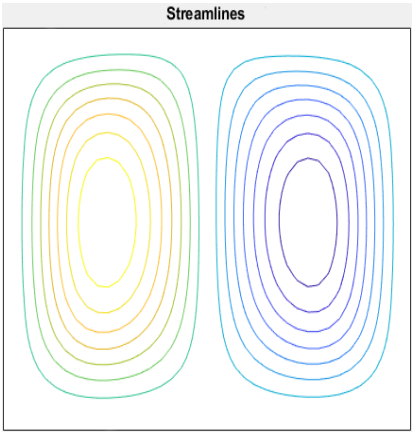

(c) -10^{-4} to 10^{-4}

Fig. 3. Solid fraction profiles, streamlines and solute concentration after 60 seconds from the start of cooling. All quantities are scaled equidistantly with yellow representing the highest value and blue the lowest value.

Figure 4 represents the macro-segregation of copper in the biphasic mixture after 14 and 22 seconds. The results of the numerical simulation indicate the presence of the two segregation zones; a positive segregation with a value superior to 4% and a negative segregation with a value inferior to 4%. The results obtained from the macro-segregation are interpreted according to the two parts (upper and lower) of the plate.

In the lower corners and bottom of the plate, negative segregation is due to sedimentation of solidified grains of low copper concentration. Next to these areas of negative segregation

are the areas of positive segregation. During cooling, zones with a concentration of more than 4% copper are formed by the flow of the liquid phase which gradually leaves this zone in order to leave space for the sedimentation of the grains.

In the same way, we note the existence of negative segregations in the upper corners still due to the phenomenon of sedimentation. The formation and accumulation of grains in the upper region involves the increase of the solid fraction, and in the course of time these grains will in turn flow downwards. Copper-rich areas, located below copper-poor areas, are formed by the movement of the melt. In the course of time, the liquid is of important volume than the solid in the upper part. The volume of the sedimented solute-poor solid will be replaced by the solute-rich liquid, thus increasing the mixing concentration.

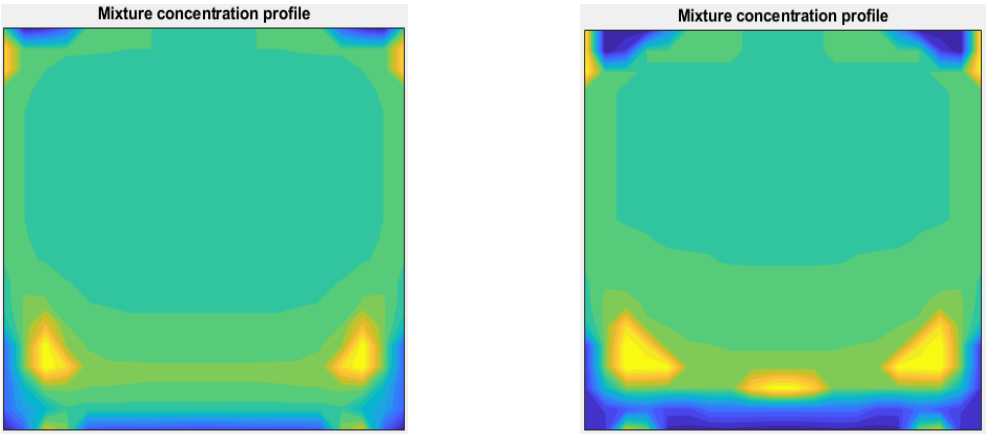

(a) t = 14 s (b) t = 22 s

Fig. 4. Evolution of macro-segregation during cooling. The highest mixture concentration is represented by the color yellow and the lowest is represented by the color blue.

4 Conclusions

In this study, the solidification of Al-4Cu alloy of almost globular equiaxed morphology was modeled. Solidification starts from the corners and the grains at these areas cannot move. On the other hand, grains away from the walls flow down the mould while increasing the solid fraction in the lower regions.

The sedimentation of the grains causes areas of negative segregation that appear in the upper corners and significantly in the lower corners and bottom of the plate. Positive segregation zones are formed next to negative segregation zones. Areas of high concentration are created by the release of the solute into the melt and its movement.

Nomenclature

c: concentration
c_p: thermal capacity
$\mathcal{C}_{sl}$: species exchange rate
d: grain diameter
f: volume fraction
f_s^c: critical solid volume fraction
g: gravity

$\mathcal{g}_\alpha$: growth factor
$\mathcal{Gr}$: number of Grashof
k: solute partition coefficient at the liquid-solid interface
L: plate length
$\mathcal{m}$: liquidus slope of the binary phase diagram
$M_{\ell s}$: mass transfer rate
$\mathcal{n}$: grain density
P: pressure
$\mathcal{Pr}$: number of Prandtl
T: temperature
$\mathcal{T}$: dimensionless temperature
$\mathcal{t}$: time
τ: dimensionless time
$\mathcal{u}, \mathcal{v}$: velocity components
$\mathcal{x}, \mathcal{y}$: cartesian coordinates
$\mathcal{X}, \mathcal{Y}$: dimensionless coordinates
ρ: density
λ: thermal conductivity
μ: viscosity
β: coefficient of thermal expansion
ψ: stream function
Ψ: dimensionless stream function
ω: vorticity
Ω: dimensionless vorticity
$\Delta\delta$: mesh size limit
Subscripts:
ℓ: liquid phase
s: solid phase
$\mathcal{m}$: mixture
$\mathcal{f}$: melting
0: initial
w: mold

References

1. M. Rappaz, P. Thévoz, Acta. Metall. **35**, 1487 (1987)
2. M. Rappaz, PH. Thévoz, Acta. Metall. **35**, 2929 (1987)
3. M. Rappaz, Int. Mater. Rev. **34**, 93 (1989)
4. J. Ni, C. Beckermann, Metall. Trans B. **22**, 349 (1991)
5. C. Beckermann, R. Viskanta, Appl. Mech. Rev. **46**, 1 (1993)
6. CY. Wang, C. Beckermann, Metall. Mater. Trans A. Phys. Metall. Mater. Sci. **27**, 2754 (1996)
7. CY. Wang, C. Beckermann, Metall. Mater. Trans A. Phys. Metall. Mater. Sci. **27**, 2765 (1996)
8. C. Beckermann, CY. Wang, Metall. Mater. Trans A. Phys. Metall. Mater. Sci. **27**, 2784 (1996)
9. A.V. Reddy, C. Beckermann, Metall. Mater. Trans B. Process. Metall. Mater. Process. Sci. **28**, 479 (1997)

10. C. Beckermann, Jom. **49**, 13 (1997)
11. J. Ni, F.P. Incropera, Int. J. Heat. Mass. Transf. **38**, 1271 (1995)
12. J. Ni, F.P. Incropera, Int. J. Heat. Mass. Transf. **38**, 1285 (1995)
13. A. Ludwig, M. Wu, Metall. Mater. Trans A. Phys. Metall. Mater. Sci. **33**, 3673 (2002)
14. M. Wu, A. Ludwig, A. Bührig-Polaczek, M. Fehlbier, P.R. Sahm, Int. J. Heat. Mass. Transf. **46**, 2819 (2003)
15. KO. Tveito, A. Pakanati, M. M'Hamdi, H. Combeau, M. Založnik, Metall. Mater. Trans A. Phys. Metall. Mater. Sci. **49**, 2778 (2018)
16. A. Pakanati, KO. Tveito, M. M'Hamdi, H. Combeau, M. Založnik, Metall. Mater. Trans A. Phys. Metall. Mater. Sci. **50**, 1773 (2019)
17. F. Ren, H. Ge, D. Cai, J. Li, Q. Hu, M. Xia, et al., Metall. Mater. Trans A. Phys. Metall. Mater. Sci. **49**, 6243 (2018)
18. M. Wu, A. Ludwig, A. Fjeld, Comput. Mater. Sci. **50**, 43 (2010)
19. M. Ishii, N. Zuber, AIChE. J. **25**, 843 (1979)
20. M. Filali, Conductivité thermique apparente des milieux granulaires soumis à des contraintes mécaniques: modélisation et mesures. Thèse, 2006
21. H. Schlichting, Boundary layer theory (McGraw-Hill, New York, 1968)